Dynamic Control of Laser-Produced Proton Beams

S. Kar,[1] K. Markey,[1] P. T. Simpson,[1] C. Bellei,[2] J. S. Green,[3] S. R. Nagel,[2] S. Kneip,[2] D. C. Carroll,[4] B. Dromey,[1] L. Willingale,[2] E. L. Clark,[5] P. McKenna,[4] Z. Najmudin,[2] K. Krushelnick,[2,*] P. Norreys,[3] R. J. Clarke,[3] D. Neely,[3] M. Borghesi,[1] and M. Zepf[1,†]

[1]*The Queen's University of Belfast, Belfast BT7 1NN, United Kingdom*
[2]*Blackett Laboratory, Imperial College, London, SW7 2BW, United Kingdom*
[3]*Central Laser Facility, Rutherford Appleton Laboratory, Chilton, OX11 0QX, United Kingdom*
[4]*SUPA, Department of Physics, University of Strathclyde, Glasgow, G4 0NG, United Kingdom*
[5]*Department of Electronics, Technological Educational Institute of Crete, Chania, Crete, Greece*

(Received 10 September 2007; published 11 March 2008)

The emission characteristics of intense laser driven protons are controlled using ultrastrong (of the order of 10^9 V/m) electrostatic fields varying on a few ps time scale. The field structures are achieved by exploiting the high potential of the target (reaching multi-MV during the laser interaction). Suitably shaped targets result in a reduction in the proton beam divergence, and hence an increase in proton flux while preserving the high beam quality. The peak focusing power and its temporal variation are shown to depend on the target characteristics, allowing for the collimation of the inherently highly divergent beam and the design of achromatic electrostatic lenses.

DOI: 10.1103/PhysRevLett.100.105004 PACS numbers: 52.38.Kd, 41.75.Jv, 41.85.Ne, 52.59.−f

Laser driven accelerators hold the promise of compact accelerating structures, which could lead to their widespread use in many applications [1,2]. After only a short period of development laser-accelerated proton beams [3,4] have been shown to have very small longitudinal and transverse emittance [5,6]. The excellent emittance is the result of a very short initial burst duration and a very small "virtual" source size. However, proton beams emerging from a laser-driven target have typically a broad energy spectrum (100% up to $E_{\max}$) and large, energy dependent, divergence angle (typically 40°–60° depending on laser and target parameters). The inherent large divergence and the energy spread can make it hard to utilize the full flux of the proton beam for applications and indeed for further transport and beam manipulation. The manipulation of laser generated proton beams gives new challenges due to the high bunch charge and short pulse nature of the beams. This means it requires innovative approaches to enable beam control—recently a technique employing electric fields triggered by a second laser pulse on a separate target, has been used for focusing selectively a portion of the beam spectrum [7]. Here we demonstrate a novel target configuration which, without the need for an auxiliary laser pulse, exploits the self-charging of the target to improve the collimation of the entire proton beam, while conserving the characteristic high laminarity required for radiography applications [8]. This approach also allows the control of chromatic properties of the beam and creation of achromatic electrostatic lenses, by exploiting the strong temporal variation of the target potential. Hence, this technique allows the full flux of the proton beam to be used in many demanding applications in science, medicine, and industry [1].

In high power laser interactions with solid targets, a significant fraction of the laser energy gets transferred to the hot electron population. Above a peak laser intensity of 10^{19} W cm^{-2}, experiments [9] and particle-in-cell simulations [10] have reported laser-to-electron conversion efficiencies up to 50%. Most of the absorbed energy is carried by the forward moving hot electron population with an electron spectrum that can be approximated as an exponential $dN/dE = (N_0/U_p)e^{-E/U_p}$, with a temperature of the order of the ponderomotive potential of the incident laser [$U_p = 0.511 \times (\sqrt{1 + (a_0^2/2)} - 1)$ MeV, where a_0 is the normalized laser vector potential]. A small fraction of the hot electron population escapes and rapidly charges the target to a potential of the order of U_p preventing the bulk of the hot electrons from escaping. The time dependence of the target potential is governed by the self-capacitance

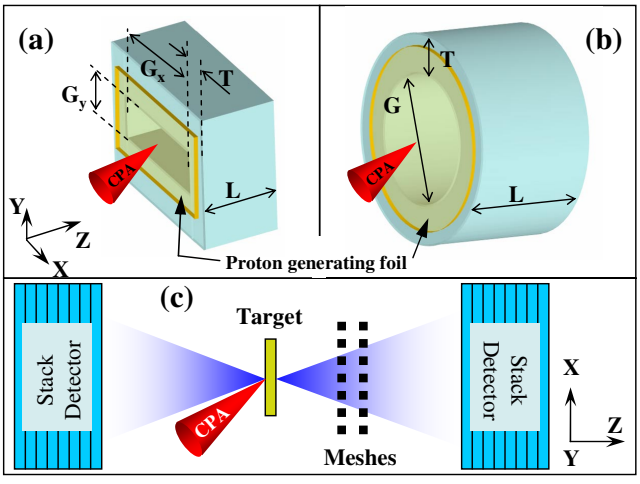

FIG. 1 (color online). Schematic of (a) rectangular and (b) cylindrical lens targets fielded in the experiment. (c) Schematic of the experimental setup (top view).

of the target (C_T). At a given time t, the number of electrons that have escaped from the target is given by $N_{es}(t) = N_0 e^{-E_{cutoff}(t)/U_p}$ which satisfies the equation, $eN_{es}(t)/C_T(t) = 10^{-6}E_{cutoff}(t)$. Here e is electron charge and E_{cutoff} is the cutoff energy (in MeV) of the confined electron spectrum. Assuming the lateral velocity of the charge wave equals to $0.75c$ [11], the time dependent target self-capacitance can be estimated as that of a disk of increasing radius $C_T(t) \sim 8\epsilon_0(r_0 + 0.75ct)$, where ϵ_0 is the permitivity of vacuum and r_0 the laser spot radius on the target. From these considerations it follows that the target potential remains above several MV for all the relevant time scales considered here. Targets charged to similar potentials have been shown to produce a substantial transverse deflections of multi-MeV proton beams [12]. Suitable design of the target geometry (as shown in Fig. 1) therefore enables a strong electrostatic lens to be created.

The experiment was performed at the Rutherford Appleton Laboratory employing the VULCAN Petawatt laser system. The laser pulse delivered ~300 J of energy on target in 500–600 fs FWHM duration. Using an $f/3$ off-axis parabola, the laser was focused to 8 μm FWHM spot with a peak intensity $\sim 10^{21}$ W cm^{-2}. Two basic shapes of electrostatic lens geometries, rectangular and cylindrical [Figs. 1(a) and 1(b)], were investigated and compared to the performance of free standing proton generating foils. The proton generating foil was 15 μm gold(Au) and the laser incidence angle was 40 degrees from the target normal. All targets were mounted on ~3 mm thick and ~2 cm long plastic stalks in order to provide a highly resistive path to the current flowing from the target to ground. Spatial and spectral profiles of the multi-MeV proton beam emitted normally from either side of the target were measured by employing stacks of radiochromic films (RCF) (a dosimetry detector [13]) as shown in Fig. 1(c). The dose response of the RCF detectors were calibrated by exposing them to various known doses of protons from a linear accelerator. In some shots, Cu sheets of suitable thickness were inserted in the stacks in order to obtain proton spectra via activation measurements [14], complementary to the spectra obtained from RCF dose measurements. Two periodic meshes were introduced at the rear side of the proton generating target, at various distances from it. Double mesh radiographs enable virtual proton source measurement [5], as well as mapping of the proton trajectories.

A significant (up to a factor of 2) reduction in the proton beam divergence angle was observed in case of the lens targets when compared to the freestanding plain foils. The angular divergence of the low energy part (up to 25 MeV) of the spectrum was observed to be highly reproducible (~56°) for the flat foil targets [typical proton beam profile is shown in Fig. 2(a)]. In order to ensure that the observed effect was unambiguously due to the target geometry, rectangular lens targets [see Fig. 1(b)] were employed. Figure 2(b) shows a 2D flux profile of the proton beam obtained from a rectangular lens target. Instead of the typical near-circular beam profile, an elliptical profile [with a major to minor axes ratio of up to 2:1 as shown in Fig. 2(b)] is observed. Only the divergence of protons that have propagated through the lens is affected (i.e., the protons propagating towards the laser are not affected by the modified target geometry). Mounting the rectangular lens on the front surface of the proton generating foil, resulted in an elliptical spatial profile of the proton beam propagating towards the laser. As expected in this case, the proton beam from the rear side of the target retains a spatial dose profile similar to that from the plain foil target. Employing lens targets with cylindrical symmetry [Fig. 1(b)], resulted in a near-circular profile of rear side protons (Fig. 3) with significant reduction in beam divergence as compared to the flat foil case.

The spectral shape and overall dose is not affected by the addition of a lens element to the target geometry. Spatially integrated proton beam spectra from both plain foil and lens targets agree to within the typical shot to shot variations. Consequently, an increase in the proton flux commensurate with the reduction in beam size is seen in the case of lens targets with respect to the plain foil case [for example, see Fig. 2(c)]. Moreover, no significant change in the proton beam cutoff energy was found in case of the lens targets in comparison to the plain foil targets. This suggests that the accelerating fields are not affected by the addition of a lens structure. This is in good agreement with expectations since the time it takes for the charge wave to spread to the lens far exceeds the proton acceleration time [11].

3D particle tracing simulations, employing PTRACE [15], were carried out in order to study the focusing due to the electrostatic lens formed by the self-charging of the target. The temporal evolution of the target potential is computed by considering the self-capacitance of a charged disk of radius $r_0 + 0.75ct$ and an exponential electron distribution with a temperature of U_P as described above. The potential of the target is assumed constant after the

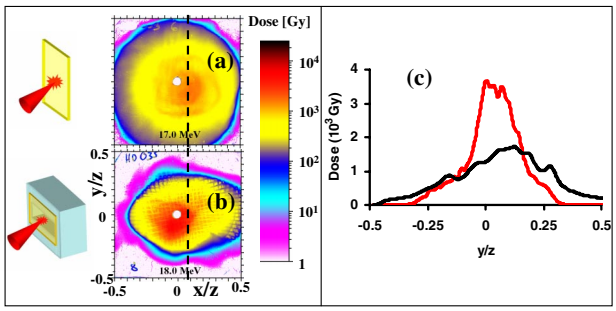

FIG. 2 (color online). Experimentally obtained proton beam (of energies ~17.5 MeV) spatial dose profiles for (a) plain foil target and (b) a Al rectangular lens target of $G_x = 5$ mm, $G_y = 1$ mm, $L = 2$ mm and $T = 0.5$ mm. Spatial scales of the images are normalized to their distances from the proton generating foil. (c) Line outs along the dotted line in (a) (black) and (b) (red) are shown.

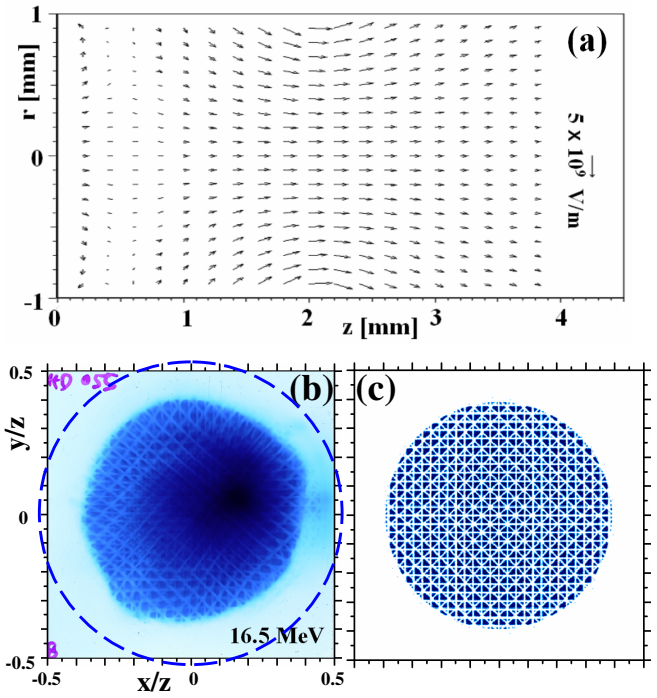

FIG. 3 (color online). (a) Longitudinal (across the XZ plane) electric field profile across a cylindrical Al lens target of $G = 2$ mm, $L = 2$ mm and $T = 0.5$ mm. Experimental (b) and simulated (c) proton spatial dose profiles (mainly due to 16.5 MeV protons) obtained from the cylindrical lens target. Spatial scales of the images are normalized to their distances from the proton generating foil. The dashed circle in (b) shows the typical proton beam size from plain foil targets.

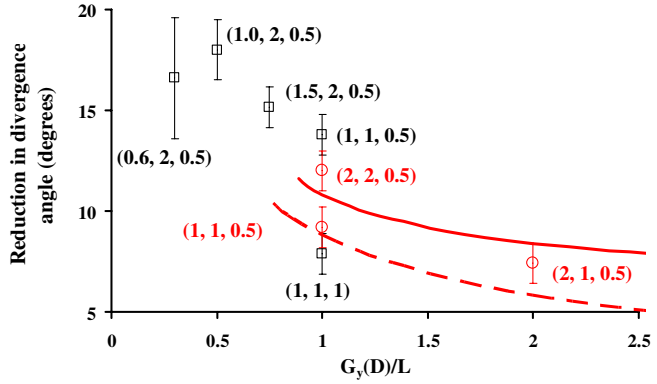

FIG. 4 (color online). Experimentally obtained data points showing reduction in proton beam (of ~17.5 MeV and ~16.5 MeV, respectively) divergence (along Y axis) due to rectangular (square) and cylindrical (circle) aluminum lens targets of different dimensions. Dimensions (in mm) of the rectangular (cylindrical) targets are mentioned as $[G_y(D), L, T]$, next to the respective data points. All rectangular lens targets had $G_x = 5$ mm. Solid (dotted) lines are simulated values for 0.5 μm thick cylindrical lens targets of G_y equals to 2 mm (1 mm).

charge wave reaches the end of the lens at a time t_{ss}, such that $r_0 + 0.75ct_{ss} = G/2 + L$ (G and L are the inner diameter and length of the cylindrical lens as shown in Fig. 1(b). The electric field at a given point and at a given time is obtained by superimposing the contributions from every part of the charged target. Test particles (protons) are launched from a point source with a divergence and position taken from the experimental observations on shots with plain foils. As shown in the Fig. 3(a), the steady state electric field profile due to a circular lens target fielded in the experiment resembles that of a conventional electrostatic *Einzel* lens and therefore acts to reduce the proton beam divergence by the strong transverse field near the edge of the charged lens target. Since the proton beam is strongly divergent inside the lens the longitudinal field also contributes to the collimation of the beam.

As shown in Figs. 3(b) and 3(c), the simulated proton beam parameters at the detector plane closely match the experimentally observed beam in both the divergence as well as the mesh magnification. Good agreement between model and observation was obtained across different energies and for all circular lens targets as shown in Fig. 4.

Both the simulations and the experimental data show that the intrinsic proton beam emittance is unaffected (to within the accuracy of our measurement). Using the method described in ref. [5], we obtained the normalized transverse emittance of the proton beam as $(0.7 \pm 0.35)\pi$ and $(0.5 \pm 0.25)\pi$ mm mrad, respectively, for the flat foil and lens-target cases. Dual mesh radiographs in the case of the lens targets confirm straight line trajectories of the proton beam outside the focusing field region.

From the comparison of simple Einzel-lens type configuration it is clear that the properties of the proton beam can be manipulated effectively. As shown in Fig. 4, collimation increases with decreasing aspect ratio G_y/L for the rectangular lens (or G/L for the cylindrical case) and decreases with increasing the wall thickness T. These effects are consistent with the higher fields obtained for a given potential for smaller structures, changes in the interaction length and variations in the target capacitance, respectively. Clearly, modifying the geometry towards more complex shapes may also yield improved collimation or focusing performance.

So far we have only discussed the behavior of the proton beam at a given proton energy. However, the focusing strength of an electrostatic lens varies strongly with beam energy—i.e. it is chromatic. Harnessing the full potential of these beams (e.g., by focusing them to one spot or coupling the whole bunch into a post accelerator or phase rotator) requires that the chromatic behavior to be addressed. The dynamic charging and discharging of the investigated structures allow a significant control of the chromatic behavior of the electrostatic lens. As the charge wave spreads at much higher speed than the protons, for the dimensions of the target used in our case, complete charging up of the target is attained much earlier than the protons leave the active focusing field region. The protons are therefore still in the field of the lens during the discharging period. The target discharges primarily due to the

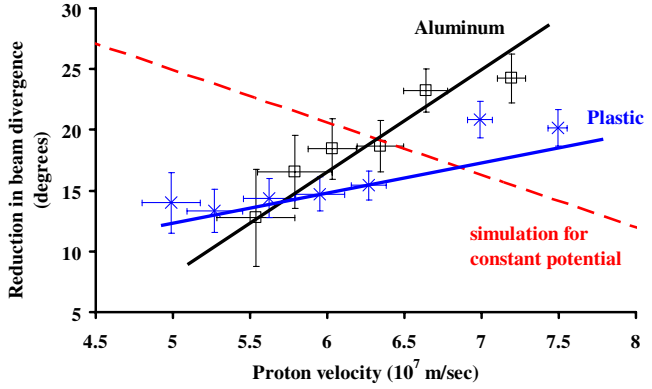

FIG. 5 (color online). Trend (solid line) of reduction in divergence over different proton beam energy for two rectangular ($G_x = 5$ mm, $G_y = 0.6$ mm, $L = 2$ mm, and $T = 0.5$ mm) lens targets of different materials, mentioned next to the respective trend lines. Red dashed line illustrates chromatic behavior of a simulated static electrostatic lens.

current flowing through the stalk holding the target. In our case, abrupt discharging of the lens target was avoided by employing the insulating stalks. The discharge time scale will also be a function of the lens material. As shown in Fig. 5 the Aluminium targets discharge (and hence lose their focusing field) much more rapidly than the plastic targets. For our geometry the discharge time constant for the Aluminium lens was roughly 7.5 ps, resulting in substantial drop of the lens potential during the particle transit. Consequently, the slower particles see a reduced collimating field and experience a smaller reduction in beam divergence. Note that for a constant potential the slower protons would experience a larger drop in beam divergence inversely proportional to the proton velocity (see Fig. 5). In the case of the plastic lens the discharge time is clearly much longer (~15 ps). In this case the slower reduction in lens potential almost perfectly compensates the enhanced collimation expected at lower energies for a constant lens potential, resulting in an achromatic collimating system. Similar approaches can be taken in order to achieve achromatic focusing or a compensation of the initial chromatic dependency of the proton beam divergence. For example mounting the target with much thinner (few microns) insulating wires is expected to result in negligible discharging of the target during the relevant time scale [16], resulting in significant improvement in lower energy proton beam collimation.

Indeed, further improvement in the beam collimation can be achieved by suitably modified lens target designs. For instance, reducing the wall thickness (T) from 0.5 mm to 50 μm will substantially increase the surface charge density. Similarly, the observed increase in beam collimation with longer L and shorter G suggests, a conical (instead of cylindrical) lens geometry will produce stronger focusing by guiding the beam optimally from its source. For example, in the case of a 30° conical lens target with initial diameter of 0.4 mm, $L = 2$ mm and $T = 50$ μm, simulations predict in excess of a factor of 3 reduction of few MeV proton beam divergence for the discussed experimental conditions. This implies an order of magnitude increase in the proton flux which would be promising for high energy density physics and fusion research. Compensating for the residual divergence (around 20°) could be achieved with a secondary lens target [7] and result in a beam collimated to a diameter of a few mm size. The use of the two combined techniques would substantially increase the scope for tuning and controlling the desired beam parameters.

In conclusion, we have shown that by careful choice of target geometry an electrostatic lens can be formed which improves the collimation of the protons emitted from a laser irradiated foil target. Significant reductions in the beam divergence and commensurate increase in flux have been observed without sacrificing the high beam quality, in excellent agreement with 3D particle tracing simulations. In addition, it is possible to offset the chromatic nature of an electrostatic lens with the discharging of the lens structure allowing for a near-achromatic lens performance and a route for correcting the chromatic aberrations inherent in the proton beam production process.

This work is funded by EPSRC. M. Zepf thanks the Royal Society for financial support. The authors acknowledge support from the target fabrication group of RAL. S. K. would like to thank Dr. A. Schiavi for the code PTRACE and T. Toncian for the RCF dose calibration.

*Present address: CUOS, University of Michigan, Ann Arbor, Michigan 48109, USA.
†m.zepf@qub.ac.uk

[1] M. Borghesi *et al.*, Fusion Sci. Technol. **49**, 412 (2006).
[2] G. Mourou *et al.*, Rev. Mod. Phys. **78**, 309, (2006).
[3] E. Clark *et al.*, Phys. Rev. Lett. **84**, 670 (2000).
[4] R. Snavely *et al.*, Phys. Rev. Lett. **85**, 2945 (2000).
[5] M. Borghesi *et al.*, Phys. Rev. Lett. **92**, 055003 (2004).
[6] T. E. Cowan *et al.*, Phys. Rev. Lett. **92**, 204801 (2004).
[7] T. Toncian *et al.*, Science **312**, 410 (2006).
[8] A. Mackinnon *et al.*, Phys. Rev. Lett. **97**, 045001 (2006).
[9] K. B. Wharton *et al.*, Phys. Rev. Lett. **81**, 822 (1998).
[10] S. C. Wilks *et al.*, IEEE J. Quantum Electron. **33**, 1954 (1997).
[11] P. McKenna *et al.*, Phys. Rev. Lett. **98**, 145001 (2007).
[12] M. Borghesi *et al.*, Appl. Phys. Lett. **82**, 1529 (2003).
[13] M. Borghesi *et al.*, Phys. Plasmas **9**, 2214 (2002).
[14] P. McKenna *et al.*, Phys. Rev. E **70**, 036405 (2004).
[15] A. Schiavi, Ph.D. thesis, Imperial College, London, 2003.
[16] S. D. Baton *et al.*, High Energy Density Phys. **3**, 358 (2007); O. Willi *et al.*, Laser Part. Beams **25**, 71, (2007).